Identification and Characterization of Small Molecule Inhibitors of the Calcium-Dependent S100B−p53 Tumor Suppressor Interaction

Joseph Markowitz,[†,‡] Ijen Chen,[§] Rossi Gitti,[†] Donna M. Baldisseri,[†] Yongping Pan,[§] Ryan Udan,[†] France Carrier,[†] Alexander D. MacKerell, Jr.,*[,§] and David J. Weber*[,†]

Department of Biochemistry and Molecular Biology, School of Medicine, University of Maryland, Department of Pharmaceutical Sciences, School of Pharmacy, University of Maryland, and MD/PhD Program, School of Medicine, University of Maryland, Baltimore, Maryland 21201

Received April 21, 2004

The binding of S100B to p53 down-regulates wild-type p53 tumor suppressor activity in cancer cells such as malignant melanoma, so a search for small molecules that bind S100B and prevent S100B−p53 complex formation was undertaken. Chemical databases were computationally searched for potential inhibitors of S100B, and 60 compounds were selected for testing on the basis of energy scoring, commercial availability, and chemical similarity clustering. Seven of these compounds bound to S100B as determined by steady state fluorescence spectroscopy (1.0 μM $\leq K_D \leq$ 120 μM) and five inhibited the growth of primary malignant melanoma cells (C8146A) at comparable concentrations (1.0 μM $\leq IC_{50} \leq$ 50 μM). Additionally, saturation transfer difference (STD) NMR experiments confirmed binding and qualitatively identified protons from the small molecule at the small molecule−S100B interface. Heteronuclear single quantum coherence (HSQC) NMR titrations indicate that these compounds interact with the p53 binding site on S100B. An NMR-docked model of one such inhibitor, pentamidine, bound to Ca^{2+}-loaded S100B was calculated using intermolecular NOE data between S100B and the drug, and indicates that pentamidine binds into the p53 binding site on S100B defined by helices 3 and 4 and loop 2 (termed the hinge region).

Introduction

S100B, a member of the S100 protein family, is a small acidic calcium-binding protein that is highly conserved and expressed in a multitude of tissues and cell lines, including astrocytes and melanocytes.[1−3] (See Appendix for abbreviations.) In general, low levels of S100B have trophic effects, and higher levels are toxic, resulting in uncontrolled cell growth.[4−7] Increased levels of S100B are found in astrocytic tumors,[8] T cell leukemia cells,[9] renal cell tumors,[10] malignant mature T cells,[11] and rat renal cell tumor lines.[10] In addition, elevated S100B levels have prognostic value for assessing the progression of malignant melanoma including recurrence of disease, disease progression to more advanced stages, and metastatic potential of the melanoma in the later stages.[12−22]

Although S100 proteins such as S100B are often referred to as markers for several cancers,[3] it is now becoming clear that S100B may contribute to cell proliferation by binding the C-terminus of p53 and inhibiting the tumor suppressor function.[23−25] While most proteins that bind or modify the C-terminus of p53 activate tumor suppression, the in vivo calcium-dependent interaction of S100B with p53 inhibits p53 tumor suppression function including reduction of p53−DNA binding and transcription activation activities.[25,26] Upon binding p53, S100B also inhibits phosphorylation of the tumor suppressor at the C-terminus[27,28] and disrupts p53 tetramers,[29] two other functions important for p53 transcriptional activity.[30] Thus, elevated levels of S100B in cancer cells such as malignant melanoma likely contribute to uncontrolled cell growth by down-regulating p53.

To better understand the S100B−p53 interaction, the 3D structures of calcium-free S100B (apo-S100B), calcium-bound S100B (holo-S100B), and holo-S100B bound to a peptide derived from the C-terminal negative regulatory domain of p53 are very useful.[24,31,32] A comparison of these three structures illustrates the details of the calcium-dependent interaction between S100B and p53.[23] Specifically, upon addition of calcium to apo-S100B, several hydrophobic residues on helix 3, helix 4, and loop 2 are exposed due to a large conformational change in the second EF-hand domain of S100B (Figure 1). It is these newly exposed residues that form a mini-hydrophobic patch on holo-S100B and participate in the S100B−p53 binding interface (Figure 1). In the absence of calcium, these same hydrophobic residues are buried in the core of an S100B subunit, and p53 cannot bind S100B, even at mM concentrations[27] (Figure 1). The availability of high-resolution structural information provides the possibility of applying structure-based approaches to identify small molecule compounds that bind to this hydrophobic patch on holo-S100B and inhibit the calcium-dependent S100B−p53 interaction.

Computer-aided drug design (CADD) offers great potential in identifying chemical compounds with a high probability of binding to a protein with a known 3D structure.[33] Database searching is a CADD approach

* Corresponding authors. D.J.W.: tel (410) 706-4354; fax (410) 706-0458; e-mail dweber@umaryland.edu. A.D.M.: tel (410) 706-7442; fax (410) 706-5017; e-mail amackere@rx.umaryland.edu.

[†] Department of Biochemistry and Molecular Biology, School of Medicine.

[‡] MD/PhD Program, School of Medicine.

[§] Department of Pharmaceutical Sciences, School of Pharmacy.

10.1021/jm0497038 CCC: $27.50
Published on Web 09/01/2004

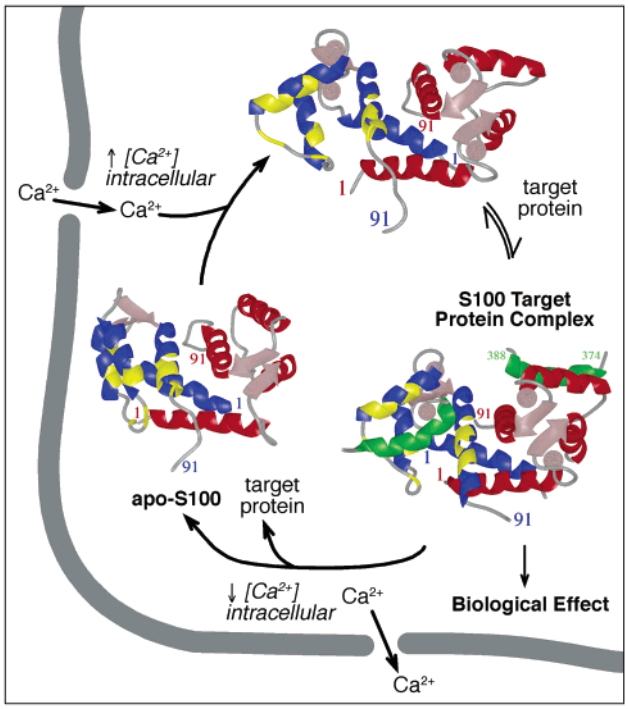

Figure 1. Amino acid residues of holo-S100B important for binding p53. The p53 binding site on holo-S100B was defined previously in a high-resolution NMR structure of holo-S100B bound to a peptide derived from the C-terminal negative regulatory domain of p53 (residues 367−388).[24] Subunits are colored blue and red, with those residues possessing NOEs to p53 colored in yellow.

that involves searching a virtual chemical database for compounds with shape, electrostatic, or other physical 3D complementarity with a selected binding site on a protein. Such an approach makes use of virtual databases containing hundreds of thousands of compounds or more from which tens to hundreds of compounds are selected for biological assay. Application of this approach has led to the identification of biologically active lead compounds for a number of systems, including inhibitors of the enzymes thymidylate synthase,[34] various proteases,[35−38] kinases,[39,40] and HIV integrase.[41] Typically, inhibitors discovered from such CADD methods have dissociation constants in the low micromolar range, and such compounds can be used as a starting point to develop molecules that bind more tightly in later cycles of drug design.

In this paper, we performed a CADD database search to identify compounds that could bind to the hydrophobic patch on S100B that interacts with p53. From the CADD search a total of 60 compounds were assayed, from which 7 where shown to have binding affinities in the μM range, and five of these compounds inhibit the growth of malignant melanoma at comparable concentrations. Furthermore, NMR techniques were used to show that these compounds bind to the p53 binding site on S100B. One such compound, pentamidine, is an FDA approved drug for protozoal diseases including treatment and prophylaxis of pneumocystis pneumonia in AIDS patients.[42] Because the pharmacology of this drug is well understood,[42] this compound was characterized further in a complex with S100B. Specifically, intermolecular NOE data between pentamidine and holo-S100B made it possible to construct a model of pentamidine bound into the p53 binding site of holo-S100B. As a future goal, the compounds identified in the present study will serve as lead compounds for the design and development of potential therapeutic agents for the treatment of cancer.

Results and Discussion

Screening for SBi*X* Inhibitors. A search for small molecules that bind S100B and prevent S100B−p53 complex formation was undertaken. The interaction between the C-terminus of p53 (residues 367−388) and S100B requires a large, calcium-dependent conformational change.[23] This change in conformation exposes several hydrophobic residues on S100B, which interact directly with p53, comprising residues in helix 2 (L35, I36), the hinge region (I47, K48), helix 3 (V52, V53, V56, M57), helix 4 (M74, V77, M79, V80, T82, A83, F87), and helix 1 from the other subunit (L3, M7).[24] On the basis of the NMR structure of p53-bound S100B, salt bridges from the C-terminus of p53 and S100B are also likely between glutamate residues (E45 and E86) of S100B and positively charged side chains of p53 (R379, K386).[24] Likewise, an inhibitory peptide, TRTK-12, binds the same hydrophobic pocket on holo-S100B using several of the same residues (L44, V52, V56, M79, V80, A83).[47] It is this hydrophobic site on S100B that was targeted in CADD screening using the program DOCK (Figure 1).

Over 640000 molecules were screened using the program DOCK, and 60 of the most promising compounds were purchased and tested for binding to holo-S100B. Of these, 21 were soluble and were suitable for fluorescent binding assays. Six compounds, SBi1, SBi2, SBi3, SBi4, SBi6, and SBi7, were found to bind S100B (1.0 μM $\leq K_D \leq$ 120 μM; Table 1) in a calcium-dependent manner as determined by fluoresecent spectroscopy (Figure 3). Furthermore, the S100B inhibitors SBi2, SBi3, and SBi7 compete directly with a peptide derived from p53 ($p53^{F385W}$), indicating that these three compounds bind to a site that at least partially overlaps with the hydrophobic patch on S100B that interacts with p53. For SBi5, binding was also observed in the absence of calcium (SBi5, $^{apo}K_D$ >20 μM), but binding to apo-S100B was significantly weaker than when calcium was present (SBi5, K_D = 4.5 ± 0.5 μM; Table 1).

One of these compounds, SBi1, is an FDA approved drug, pentamidine isethionate, and was found to bind to S100B with a relatively high affinity (K_D=1.0 ± 0.6 μM; Figure 3). (The isethionate salt was chosen for this study because it is FDA approved; the mesylate salt is diabetogenic and is not approved for use in the United States.) In addition, pentamidine isethionate (SBi1) inhibits human primary malignant melanoma cell growth (IC_{50} = 1.2 ± 0.3 μM; Table 1) in a concentration range comparable to its binding constant to S100B (K_D = 1.0 ± 0.6 μM; Table 1). Lesser effects from SBi1 treatment (>9-fold) were observed on the growth of normal melanocytes. While these results are consistent with the idea that p53 activity is restored by inhibiting the S100B−p53 interaction, other mechanisms for inhibiting cell growth cannot be completely ruled out in this case or for the other inhibitors that inhibit cell growth such as SBi3, Sbi4, SBi5, and SBi6 (Table 1). For SBi2

Table 1. Binding to Holo-S100B, Saturation Transfer Differences, and Inhibition of Primary Malignant Melanoma Cell Growth for Seven SBi*X* Inhibitors

X in SBi*X*	K_D (μM)	STDs[e]	IC_{50} (μM)
1	1.0 ± 0.6[a,b]	H2/H5 ≈ H3/H6, α, $\beta \approx \gamma$	1.2 ± 0.2[f]
2	4.5 ± 2.3[c]	ϕ_1(H2/H6; H3/H5, H4), ϕ_2(H2/H6; H3/H5) ($N1CH_3$, CH_3); α, β, NH	>100[g]
3	120 ± 17[c,d]	mesityl(H3/H5, (4-CH_3 > 2/6-CH_3)), isophthalic acid(H2/H6 < H4), isoindol ((H4), H5 < H6)	44 ± 11[h]
4	2.0 ± 0.2[b]	H4 ≈ H5 ≈ H6	8.0 ± 3.0[i,f]
5	4.5 ± 0.5[a]	limited solubility	12.0 ± 4.0[i]
6	18.3 ± 4.4[a]	ϕ_1(H6 > H2,H5), ϕ_2(H3 ≈ H4, H6), furyl(H3 ≈ H4)	49 ± 16[i]
7	8.1 ± 1.0[c,d]	ϕ_1(H6), (H5 > H4,H2), dioxosionindoline (H3 > H4, H6); *tert*-butyl ≈ ϕ_1(H5), NH	>100[g]

[a] Intrinsic fluorescence of compound was monitored during titrations with holo-s100B. [b] The emission of the tryptophan residue in F43W S100B bound to the small molecule inhibitor was monitored in competition studies with wild-type S100B. The dissociation constants of SBi1 ($K_D = 0.9 \pm 0.2$ μM) and SBi4 ($K_D = 0.6 \pm 0.1$ μM) from F43W S100B were used together with the apparent dissociation constant (K_{app}) from the competition titration to calculate the dissociation constant from wild-type S100B using $K_D = K_{app}/(1 + [\text{F43W S100B}]/{}^{F43W}K_D)$. [c] The emission of the tryptophan residue in the $p53^{F385W}$ peptide bound to wild-type S100B was monitored in competition studies with the small molecule inhibitor. The dissociation constant of the $p53^{F385W}$ peptide from wild-type S100B ($^{p53F385W}K_D = 5.6 \pm 1.0$ μM[27]) was used together with the apparent dissociation constant (K_{app}) from the competition titration to calculate the dissociation constant of the inhibitor from wild-type S100B using $K_D = K_{app}/(1 + [p53^{F385W}]/{}^{p53F385W}K_D)$. [d] Tyrosine fluorescence of wild-type S100B was monitored during the titrations. [e] Naming of protons and functional groups for each compound are illustrated in Figure 1 and in the Experimental Section. Comparisons are valid only in cases in which the longitudinal relaxation rates (T_1) are similar (i.e. within 10%) as previously described.[65] [f] The two highest affinity compounds were also tested for their ability to inhibit the growth of normal melanocytes. A lesser effect on the growth of normal melanocytes was observed for both SBi1 (>9-fold) and SBi4 (>4-fold), compared to their effect on growth of primary malignant melanoma cells. [g] SBi2 and SBi7 are soluble in aqueous solution when bound to holo-S100B, but they did not affect cell growth. These results are most readily explained by the fact that these two compounds do not enter efficiently into cells. [h] SBi3 was found to have a more toxic effect on cell growth than can be explained by its affinity for S100B; thus, this molecule must also bind some other protein(s) and/or DNA that affects the growth rate of malignant melanoma cells. [i] The inhibitors SBi4, SBi5, and SBi6 all inhibit cell-growth; however the IC_{50} values for these compounds are at concentrations 2−3-fold higher than their dissociation constants for S100B. Decreased potency may be caused by sequestration of the inhibitor into cellular compartments, metabolism of the compound itself, and/or by some other unknown mechanism(s).

and SBi7, the inability to enter cells is suggested to be the reason for their inability to inhibit cell growth (Table 1).

Screening Compounds Using Saturation Transfer Difference NMR. Saturation transfer difference (STD) NMR experiments were used to identify protons of the small molecule inhibitors that are at the SBi*X*−S100B binding interface as previously described for other protein−ligand complexes[64,65] (Table 1). Specifically, qualitative conclusions pertaining to the relative proximity of protons on the inhibitor to those on the protein and epitope mapping of the inhibitor can be achieved when STD data for protons or groups of protons of comparable longitudinal relaxation times (T_1) are compared.[65] Furthermore, STD data such as this can be considered when evaluating models of inhibitor−protein complexes that are calculated with more rigorous methods for structure determination.

For calcium-loaded S100B, STD NMR was readily applicable to the lower affinity S100B−SBi*X* complexes ($K_D > 5$ μM), such as for SBi3, SBi6, and SBi7, because of their fast exchange kinetics.[64] Despite the relatively high affinity of SBi1, SBi2, and SBi4 −SBi7 for S100B ($K_D < 5$ μM; Table 1), it was possible to detect saturation transfer differences for these compounds by increasing the concentration of excess inhibitor as previously described[64] (Figure 4). For SBi5, no STDs could be measured because the SBi5−S100B complex has very limited solubility.

The tight binding inhibitors ($K_D < 10$ μM; SBi1, SBi2, SBi4, SBi7) give STDs to both aliphatic and aromatic protons throughout the molecule, indicating that multiple protons on the inhibitor are proximal to protons on S100B. In the case of the weaker binders ($K_D > 10$ μM; SBi3, SBi6), STDs to some regions of the molecule were not observed or very weak, suggesting that these regions are less important for binding to S100B. In the case of SBi6 ($K_D = 18.3 \pm 4.4$ μM; Table 1), STDs are observed on both substituted aromatic rings (ϕ1, H2, H5, H6; ϕ2, H2, H3, H5) and on the furan ring (H3, H4). However, the absence of STD to the carbon-bound hyrdazone proton (i.e. proton attached to the carbon adjacent to the furan group) is evidence that this region of SBi6 is further away from protons of holo-S100B. The weakest binding inhibitor, SBi3 ($K_D = 120 \pm 17$ μM; Table 1), is probably anchored into holo-S100B with an aromatic group, only in this case it is the mesityl moiety that provides the largest STDs with smaller STDs observed for protons on the isophthalic and isoindol groups.

Mapping the Inhibitor-Binding Site on Holo-S100B. Titrations of S100B with the inhibitors (SBi1−SBi7) were monitored using HSQC NMR spectra to map their binding sites on S100B. While chemical shift perturbations of amide−proton correlations ($^{15}N-H_N$) can sometimes result from more global structural changes upon complex formation, such information, as a whole, is often very useful for identifying the general location of where small molecules bind to proteins.[78,79] In this study, the chemical shift assignments of S100B could be adequately made by keeping track of the perturbations during titrations with SBi2, SBi3, SBi4, and SBi6. However, for SBi1 and SBi7, it was necessary to confirm such assignments made during the titration using sequential NOE data from 3-dimensional NOE data (αN, βN, NN, etc.) as previously described.[80] In one case (for SBi5), however, the inhibitor complex with S100B was relatively insoluble at NMR concentrations (>100 μM), and the chemical shift perturbations could not be unambiguously assigned. Overall, titrations with six of the seven inhibitors of S100B (SBi1, SBi2, SBi3, SBi4, SBi6, SBi7) caused significant perturbations in both proton and nitrogen chemical shift values of holo-S100B in the hinge region (residues L40−E46), in helix 3 (residues E51−V53, M57, T59−L60), in helix 4 (residues E72, M74−A75, V77−M79, T82−C84), and in the C-terminal loop (F87−H90), which significantly

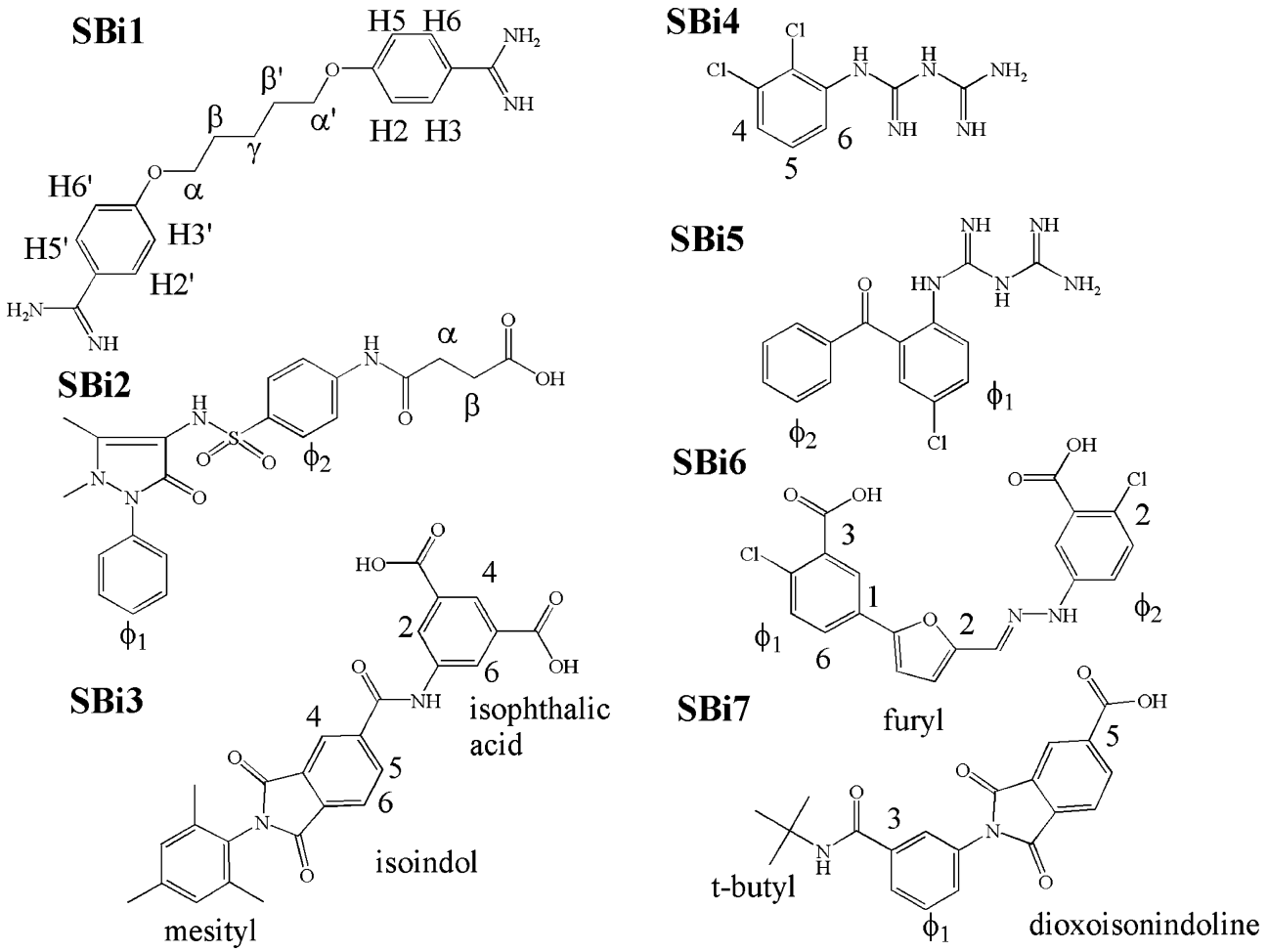

Figure 2. Inhibitors of the holo-S100B−p53 peptide complex. The IUPAC names of the inhibitors SBi1−SBi7 are given in the Experimental Section. Numbering and names to chemical moieties are illustrated in this figure to facilitate the discussion of the compounds.

overlaps the region of S100B responsible for binding p53 and TRTK-12 (Table 2; Figure 5A). Control experiments, in the absence of calcium, showed none of these six compounds to exhibit H_N or ^{15}N chemical shift perturbations consistent with the calcium dependence of these S100B−inhibitor interactions. For SBi5, small chemical shift changes were also observed in the hinge region of S100B in the absence of calcium, which is consistent with fluorescent data that showed binding of this compound to both apo-S100B (weak binding) and holo-S100B.

NMR-Docked Model of Pentamidine (SBi1) Bound to Holo-S100B. While chemical shift perturbations and saturation transfer difference NMR can be used in a qualitative manner to map binding epitopes on holo-S100B and SBi1, respectively, it is important to obtain direct evidence for intermolecular proximities to accurately characterize binding at the S100B−SBi1 interface. In this regard, intermolecular NOEs were assigned between protons of SBi1 and aromatic residues of calcium-loaded S100B (F73, F76, and F88; Figure 5B). These intermolecular NOE correlations were then used to dock SBi1 into the NMR structure of Ca^{2+}-S100B[32] using methods described previously[72,73] (Figure 5B). The resulting model (Figure 6) was found to be consistent with nearly all of the HSQC perturbation and STD data. For example, HSQC perturbations are observed for helix 1, the hinge region, helix three, helix four, and the C-terminal loop consistent with the NMR-docked model that places SBi1 into the p53 binding site on S100B defined by helices 3 and 4 and loop 2 (termed the hinge region). Smaller HSQC pertubations were observed in helix three upon the addition of SBi1, which could not be easily explained by the location of the inhibitor in the NMR-docked model; however, such smaller chemical shift perturbations could also result from a slight reorientation of this helix upon the addition of SBi1. Nonetheless, it is clear from this NMR-docked model (Figure 6) that SBi1 binds a region of holo-S100B that overlaps significantly with the p53 binding site illustrated in Figure 1.

Conclusions. Novel inhibitors of the S100B−p53 peptide complex were obtained using a combination of computational chemistry, structural biology, and molecular biological approaches. These seven compounds represent the first round of a rational drug design project targeting the identification of inhibitors of the protein S100B. In one case, we have found an FDA approved drug, pentamidine isethionate, which binds to the p53 binding site on S100B. Future efforts will involve developing such lead compounds into higher affinity inhibitors of S100B, which could potentially have useful cancer therapeutic properties.

Experimental Section

Materials. All chemical reagents were ACS grade or higher unless otherwise indicated. Buffers were passed through

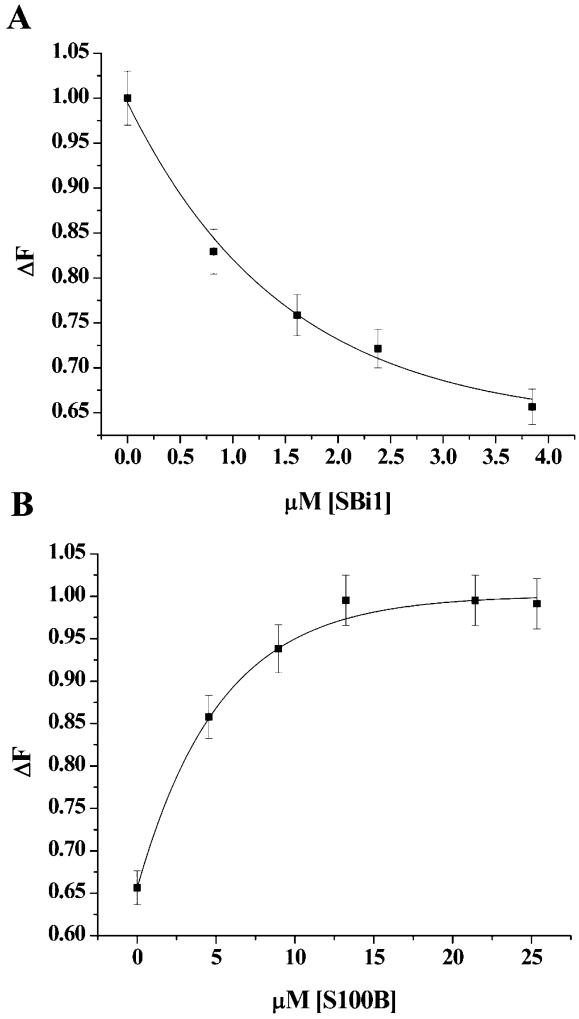

Figure 3. Binding studies of pentamidine isethionate to holo-S100B. (A) Titration of pentamidine isethionate (SBi1) into a solution containing 4 μM F43W S100B, 100 mM KCl, 10 mM $CaCl_2$, 40 mM tris, 25 °C, pH 7.5. (B) Titration of wild-type S100B into a solution containing SBi1 bound to F43W S100B. In these titrations, the concentrations of F43W and pentamidine isethionate were kept constant throughout the titration.

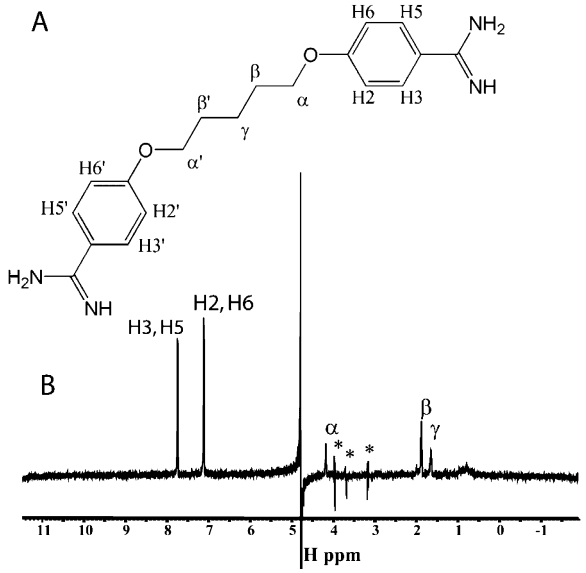

Figure 4. Saturation transfer difference data for pentamidine bound to holo-S100B. (A) Chemical structure of pentamidine shown together with labels for the aliphatic and aromatic protons of the compound. (B) STD spectra for pentamidine isethionate bound to holo-S100B illustrating that all of the protons of pentamidine are in proximity to protons in holo-S100B. Conditions included 0.15 mM S100B, 1.5 mM pentamidine, 30 mM Tris, 1 mM DTT, 0.4 mM EDTA, 10 mM $CaCl_2$, 100 mM KCl, 0.3 mM NaN_3, 5% D_2O, pH 7.5, 25 °C. Peaks labeled with an asterisk (*) are subtraction artifacts arising from the isethionate salt and Tris-HCl buffer in the sample.

Chelex-100 resin (Bio-Rad) to remove trace metals. Perdeuterated Tris, d_{11}-Tris (1 M solution in D_2O), D_2O, and $^{15}NH_4Cl$ were purchased from Cambridge Isotope Laboratories, Inc. Small molecules screened for binding to S100B were purchased from Sigma, Ryan Scientific Inc. (Maybridge Database), and Hit2lead (Chembridge Database; www.hit2lead.com).

Computational Methods. The program DOCK 4.0.1[43,44] was used to screen a virtual small molecular weight library of approximately 640000 compounds, that was prepared as previously described.[45,46] Database screening targeted a hydrophobic pocket on p53 peptide-bound S100B from which the peptide was removed.[24,32] Residues in this same hydrophobic site also provided numerous interactions to the TRTK peptide.[47] Screening via DOCK used flexible ligands based on the anchored search method.[48] The solvent accessible surface on S100B was calculated using the program DMS,[49] and sphere sets were chosen with the DOCK associated program SPHGEN,[50,51] which places target spheres in concave regions of the solvent accessible surface. Of these spheres, those in proximity (<14 Å) of all amino acid residues important for S100B−p53 interactions (residues L44, K48, E51, V52, K55, V56, V77, V80, T82, A83) were selected to define the target site.[24] The program SYBYL (Tripos Inc.) was used to assign partial charges to the protein, including those on calcium. For calculation of interaction energies, the grid method was applied,[52,53] using a GRID with box dimensions 30 × 31 × 36 Å^3 based on the edges being 10 Å beyond the position of the selected spheres. Scoring of compounds was based on the van der Waals attractive term,[46] even though the ligand buildup procedure in DOCK is based on the full interaction energy. Use of the vdW attractive term for scoring ensures that compounds that have steric complementarity with the binding regions are selected, avoiding the selection of compounds dominated by electrostatic interactions that may potentially be nonspecific.[46]

Four groups of compounds were screened using DOCK: group I includes ≈180000 compounds from the National Cancer Institute (NCI) database (Milne 1994); group II includes ≈350000 compounds from the Maybridge, Chembridge, Asinex, Indexnet, Idxchmcs, and Menai databases; group III includes ≈70000 compounds from the Sigma database; and group IV includes ≈40000 compounds from the Derwent World Drug Index. In the screen of the NCI database (group I), the top scoring 600 compounds were tabulated and evaluated further. Of these 600 compounds, five were chosen for binding studies based upon current knowledge of the p53 binding site on S100B,[24] likeness to known drug scaffolds, and commercial availability.

For group II, the top scoring 20000 compounds were subjected to a second, more rigorous DOCK search involving several rounds of energy minimization and additional structural optimization.[46] From this second DOCK search, the top 500 compounds were tabulated and evaluated on the basis of solubility, potential toxicity, and likeness to known drug scaffolds. To increase the likelihood of obtaining active compounds, these top 500 compounds were also subjected to ChemFinder chemical similarity clustering to maximize the structural diversity of compounds for assay.[54] Thirty-nine compounds from various clusters were assayed using steady state fluorescence and NMR spectroscopy techniques. In addition, if any of the compounds demonstrated similarities with pentamidine (from original DOCK search; group I), then it too was chosen for binding studies. The screening of the Sigma (group III) and Derwent (group IV) databases was treated in an analogous manner to that of the NCI database (group I) except that an additional screen was performed for

Table 2. Chemical Shift Perturbations for Residues in Holo-S100B upon the Addition of Inhibitors (SBi*X*)[a]

X in SBi*X*	helix 1	loop 2 (hinge)	helix 3	helix 4	C-terminal loop
1	A9 I11 F14 H15	S41 L44 E45 E46	V52 T59	M74 A75 V77 A83	E89 H90
2[b]		H42 F43 L44	V51 V56 L60 C68	E72 V77 S78 M79 T81 T82 A83 C84 H85	E86 E91
3[c]	L3 Ill D12 V13 F14 S18	S41 E46 K48 E49	E51 T59	E72 M79 A83	E89 H90
4	L3 A9 H15 Y17 S18	L44 E45	M57 T59	V77 A83	F88 H90
5[d]					
6		F43 F44		E72 A83	E89 H90
7[e]	F14	L40 F43 E45	V52 V53	T82	F88
TRTK[f]		L40 H42 L44 E45 I47	V52 K55 V56 T59	M79 V80 A83 C84	F87
p53[f]		L44	V52 V56	M79 V80	F87

[a] Mapping of the binding site on holo-S100B using chemical shift perturbations ($\Delta\delta^1H + \Delta\delta^{15}N$) for residues on S100B upon addition of SBi*X*. [b] SBi2 also shows changes in chemical shift for residues in the second β sheet (C68). [c] SBi3 also shows changes in chemical shift for residues in the first loop (H25) second β sheet (D69). [d] SBi5 complexed with holo-S100B was minimally soluble at concentrations necessary for NMR (>100 μM), so no chemical shift assignment could be unambiguously made for this compound when bound to holo-S100B. [e] SBi7 also shows changes in chemical shift for residues in helix 2 (N38). [f] Residues for which intermolecular NOEs are observed for the TRTK−holo-S100B complex and the p53−holo-S100B complex. For the TRTK-12 peptide, intermolecular NOE correlations to I36 in helix 2 are also observed.

chemical similarity against the inhibitors discovered previously in the group I and II searches.

In total, 60 compounds identified using DOCK were purchased from Sigma, Ryan Scientific Inc. (Maybridge) or Chembridge Corporation. Of these 60 compounds, 7 were found to be soluble and bind S100B in the p53 site. These compounds were named S100B inhibitors 1−7, SBi*X* (X = 1−7), and are presented in Figure 2. SBi1: pentamidine isethionate (Sigma-Aldrich, St. Louis, MO). SBi2: 4-[(4-{[(1,5-dimethyl-3-oxo-2-phenyl-2,3-dihydro-1*H*-pyrazol-4-yl)amino]sulfonyl}phenyl)-amino]-4-oxobutanoic acid (Ryan Scientific Inc., Isle of Palms, SC). SBi3: 5-{[(2-mesityl-1,3-dioxo-2,3-dihydro-1H-isoindol-5-yl)carbonyl]amino}isophthalic acid (Hit2lead.com, San Diego, CA). SBi4: *N*-(2,3,dichlorophenyl)imidodicarbonimidic diamide (Ryan Scientific Inc., Isle of Palms, SC). SBi5: *N*-(2-benzoyl-4-chlorophenyl)imidodicarbonimidic diamide hydrochloride (Ryan Scientific Inc., Isle of Palms, SC). SBi6: 5-((2*E*)-2-{[5-(3-carboxy-4-chlorophenyl)-2-furyl]methylene}hydrazino)-2-chlorobenzoic acid (Hit2lead.com, San Diego, CA). SBi7: 2-{3-[(*tert*-butylamino)carbonyl]phenyl}-1,3-dioxoisonindoline-5-carboxylic acid (Hit2lead.com, San Diego, CA) (Figure 2). The IUPAC names for the inhibitors were obtained using a program from the Advanced Chemistry Development I-Lab service (v. 7.06; ACD, www.acdlabs.com).

Solubility Trials. Each of the 60 compounds purchased for the experimental screening was first dissolved in deuterated DMSO (99.96%; Cambridge Isotopes) and then tested for solubility in aqueous buffers. For those compounds with significant solubility, their relative solubility was tested further in the presence of holo-S100B using the hanging drop technique and various conditions as previously described.[55] The chemical literature of related small molecules bound to either protein or DNA was also searched to obtain possible conditions to solubilize the S100B−inhibitor complexes; such was the case with inhibitor SBi1 where the dilution in water first and the inclusion of 100 mM KCl were found to be critical for its solubility as found previously in other systems.[56]

Inhibition of Cell Growth. Primary malignant melanoma cells (C8146A) were obtained from Dr. Frank L. Meyskens (University of California, Irvine) and were plated at a density of 10000 cells per well in 24-well plates containing F10 media (10% FBS). The following day, the original growth media was removed and replaced with fresh F10 media (10% FBS) containing the various compounds, in quadruplicate trials, at six concentrations. As a control, cell growth was also monitored in media without compound but containing DMSO. Five days after addition of the compounds, cell viability was analyzed using a standard MTT assay as previously described.[57] In this assay, the compound-containing media was removed and the cells were treated with methyldiazoletetrazolium (MTT, 0.25 mg/mL in PBS) for 3 h at 37 °C. The unreacted solution was then removed, and 1 mL of 100% DMSO was added to solubilize the MTT−formazan product. Quantification of violet crystals reflecting cellular growth and viability was determined by absorbance at 540 nm relative to the controls done in the absence of compound.

Normal melanocytes were purchased from Cell Applications, Inc. (San Diego, CA), and were plated at a density of 10000 cells per well in 24-well plates containing MEM growth medium purchased from Cell Applications, Inc. The following day, the original growth media was removed and replaced with fresh MEM growth media containing SBi1, SBi4, or no compound in quadruplicate trials at several concentrations (1−25 μM). Cells were removed from the surface of the wells 5 days after the addition of the compounds. The excess media was removed via washing with 0.4 mL of HBSS per well. Following the washing step, addition of 0.2 mL of trypsin (until cells visibly detach from surface) was followed by addition of 0.5 mL of trypsin neutralizing solution and 0.5 mL of HBSS. Cells were counted using a hemocytometer.

Fluorescence Spectroscopy. Compounds were tested for binding to holo-S100B using fluorescence spectroscopy (SBi1−SBi7; Figure 2). Unless otherwise stated, conditions for fluorescence binding assays included 40 mM Tris, 10 mM $CaCl_2$, 100 mM KCl, 25 °C, pH 7.5. KCl was not included in titrations with SBi2 and SBi7. For the three fluorescent compounds discovered to bind S100B (SBi1, SBi5, SBi6), the change in the compound's fluorescence intensity was measured during titrations with S100B. Three other approaches to characterize binding were used for those compounds that are not fluorescent (SBi2, SBi3, SBi4, SBi7) or weakly fluorescent (SBi1). First, the changes in tyrosine fluorescence of S100B upon the addition of the small molecule were monitored in titrations with compounds SBi3 and SBi7. Second, the emission of an S100B tryptophan mutant (F43W) was monitored during titrations with the compounds SBi1 and SBi4. After this titration, wild-type S100B (contains no tryptophan) was used to compete with a tryptophan-containing mutant (F43W), and the fluorescence intensity of F43W S100B was restored in each case. Typical conditions in these titrations included 4 μM F43W S100B, 10 mM $CaCl_2$, 40 mM Tris-HCl, 100 mM KCl, 25 °C, pH 7.5. A third method made use of a fluorescent peptide derived from p53 (F385W) that binds holo-S100B (K_D = 5.6 ± 1.0 μM).[27] In these competition assays, the addition of compounds SBi2, SBi3, and SBi7 to the S100B−p53 complex restored the fluorescent intensity of $p53^{F385W}$ peptide; K_D values were then calculated using $K_D = K'/(1 + [p53^{F385W}]/{}^{p53F385W}K_D)$ where K' is from the best-fit curve of the titration data and a ${}^{p53F385W}K_D$ value of 5.6 ± 1.0 μM.

Steady-state experiments to determine binding constants were performed on an Aminco Bowman series 2 luminescence spectrophotofluorometer with the temperature of the cell (quartz cuvette) maintained at 25 °C. In all cases, the binding constant was obtained from titrations performed with at least two different concentrations of the fluorophore (compound, wild-type S100B, F43W S100B, and/or $p53^{F385W}$ peptide).

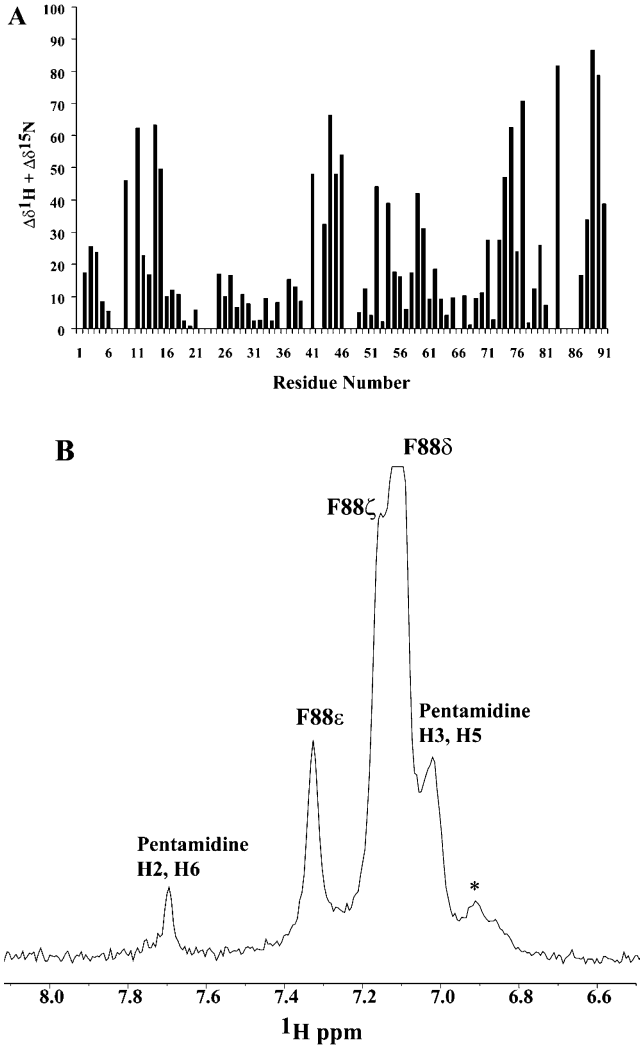

Figure 5. Chemical Shift perturbations and intermolecular NOE correlations arising from pentamidine bound to holo-S100B. (A) HSQC difference map illustrating ^1H and ^{15}N perturbations upon addition of pentamidine to holo-S100B. Conditions included 0.75 mM S100B, 1.0 mM pentamidine, 30 mM Tris, 5 mM DTT, 0.4 mM EDTA, 10 mM $CaCl_2$, 100 mM KCl, 0.3 mM NaN_3, 5% D_2O, pH 7.5, 37 °C. (B) 1D slice (t_2) from a 2D NOESY experiment illustrating intermolecular NOE correlations between F88δ protons of Ca^{2+}-loaded S100B (diagonal) and protons of pentamidine. Also labeled are intraresidue NOE correlations to F88ϵ and F88ζ protons. While the intermolecular NOE to the H2/H6 protons of pentamidine is unambiguous and without overlap, the intermolecular NOE labeled for the H3/H5 protons overlaps with other intramolecular NOEs to F88δ. The peak labeled with an asterisk (*) is not maximized in this slice of the 2D spectra. Conditions included 0.5 mM S100B, 1.0 mM pentamidine, 30 mM Tris, 5 mM DTT, 0.4 mM EDTA, 10 mM $CaCl_2$, 100 mM KCl 0.3 mM NaN_3, D_2O, pD 7.5, 37 °C.

NMR Spectroscopy. NMR spectra were acquired at 25 °C and/or at 37 °C with a Bruker Avance 600 MHz and a Bruker Avance 800 MHz NMR spectrometer each equipped with four frequency channels and a triple resonance 3-axis gradient probe. Data were processed on Linux workstations using the processing program nmrPipe [58] or nmrView.[59] The backbone and side chain chemical shifts of Ca^{2+}-loaded S100B and S100B bound to p53 peptide have been described previously.[24,32] The assignments of ^{15}N-labeled S100B bound to the compounds could be made in most cases from titration of the compounds into Ca^{2+}-S100B as monitored by a 2D $^1H-^{15}N$ fast HSQC.[60] Three-dimensional NOESY−HSQC data were necessary to confirm the assignments of S100B bound to SBi1 and SBi7. NMR sample conditions typically consisted of 0.1−1.0 mM S100B, 0−2.5 mM compound, 30 mM Tris-HCl, 100 mM KCl, 10 mM $CaCl_2$, 0.3 mM NaN_3, 0.4 mM EDTA, 5 mM DTT, 5% D_2O, and pH 6.5−7.5. For SBi1 bound to unlabeled holo-S100B, a 2D presat NOESY (150, 200, and 300 ms mixing time), and a 2D presat TOCSY (71 ms spin-lock time) were collected in D_2O. For these experiments, conditions included 0.5 mM S100B, 1.0 mM pentamidine, 30 mM Tris-HCl, 1 mM DTT, 0.4 mM EDTA, 10 mM $CaCl_2$, 100 mM KCl, 0.3 mM NaN_3, D_2O, pD 7.5, 37 °C.

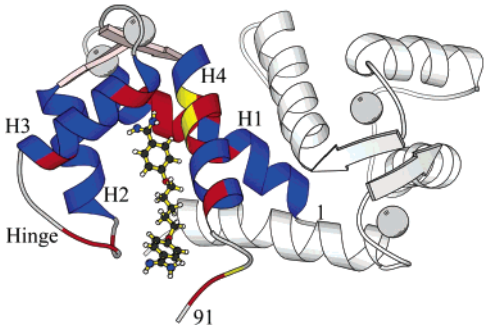

Figure 6. Ribbon diagram of the NMR-docked model of pentamidine (SBi1) bound to holo-S100B. Subunits of the S100B dimer are shown in blue and gray with residues that have HSQC perturbations colored in red, and residues that have intermolecular NOEs to their aromatic side chains colored in yellow (F73, F76, F88).

To verify the calcium dependence of the small molecule interaction between each of the compounds (SBi1−SBi7) and S100B, HSQC spectra were collected both in the presence and in the absence of calcium. In cases where sample conditions were changed, a control Ca^{2+}-S100B HSQC spectrum was collected under the new conditions, which was sufficient to verify the assignments in all cases since very minor changes in chemical shift were observed. All proton chemical shifts are reported with respect to the H_2O or HDO signal taken as 4.658 ppm relative to external TSP (0.0 ppm) at 37 °C; 4.773 ppm relative to external TSP (0.0 ppm) at 25 °C. The ^{15}N chemical shifts were indirectly referenced using the following ratio of the zero-point frequencies at 37 °C and 25 °C: 0.10132905 for ^{15}N to ^1H.[61−63]

Candidate inhibitors (including SBi1−SBi7 and others) were subjected to group epitope mapping via saturation transfer difference (STD) NMR.[64] The duration of the presaturation period (1 s to 8 s) for STD experiments was optimized as previously described.[64] As a control, the STD experiments were collected in the absence of a $T_{1\rho}$ filter and as expected the 1D spectrum of holo-S100B was fully restored. STDs were collected at 25 °C, due to more efficient saturation of the protein at the lower temperature (i.e. versus 37 °C) as previously described.[65] Typical sample conditions included 75−150 μM S100B, 30 mM Tris, 1 mM DTT, 0.4 mM EDTA, 10 mM $CaCl_2$, 100 mM KCl, 0.3 mM NaN_3, 5% D_2O, pH 7.5, 25 °C; 1.5−3.0 mM SBi*X*. All samples for the STD experiments were prepared with the compounds in 10−30-fold molar excess of Ca^{2+}-S100B, and the proton assignments of the compound were made using NMR experiments including standard 1D Watergate,[66] 1D selective NOESY (GOESY),[67] 1D selective decoupling experiments, 1D inversion recovery experiments (T_1), and 2D TOCSY (spin-lock times of 5 ms to 72 ms),[68] 2D NOESY,[69] and 2D HMBC[70,71] experiments.

Modeling of the Holo-S100B−SBi1 Complex. Intermolecular NOE correlations between SBi1 and holo-S100B were used to orient SBi1 into the previously determined NMR structure of Ca^{2+}-S100B [32] to give an NMR-docked model of the S100B−SBi1 complex using previously described methods.[72,73] SBi1's chemical shifts were confirmed via titration of S100B into a 100 μM SBi1 sample using a standard 1D Watergate.[66] Specifically, coordinates for SBi1 were formatted for use in XPLOR with the program XPLO2D[74] and 20 steps of Powel minimization were applied to SBi1 in XPLOR prior

to docking it into S100B. Next, simulated annealing refinements were run, which made use of all the NOE and dihedral angle constraints including intermolecular NOE correlations between SBi1 and S100B, using the program XPLOR-NIH.[75] The resulting models were visualized using the program VMD-XPLOR,[76] and figures were produced with MIDAS[49] and MOLSCRIPT.[77]

Acknowledgment. This work was supported by grants from the National Institutes of Health (GM58888, to D.J.W.; F30-NS043916, to J.M.; CA095200 to A.D.M.), from the University of Maryland, School of Pharmacy, and Computer-Aided Drug Design Center, MD/PhD Program, and from the American Cancer Society (RPG0004001-CCG) to D.J.W.

Appendix

Abbreviations. S100β, subunit of dimeric S100B; NOE, nuclear Overhauser effect; NMR, nuclear magnetic resonance; HSQC, heteronuclear single quantum coherence; NOESY, nuclear Overhauser effect spectroscopy; TOCSY, total correlation spectroscopy; STD, saturated transfer difference; GOESY, gradient Overhauser exchange spectroscopy; COSY, correlation spectroscopy; HMBC, heteronuclear multi bond correlation; SBi*X*, S100B inhibitor number *X*.

References

(1) Zimmer, D. B.; Cornwall, E. H.; Landar, A.; Song, W. The S100 protein family: history, function, and expression. *Brain Res. Bull.* **1995**, *37*, 417−429.
(2) Zimmer, D. B.; Wright, P.; Weber, D. J. Molecular mechanism of S100-target protein interactions. *J. Microsc.* **2003**, *324*, 1003−1014.
(3) Heizmann, C. W.; Fritz, G.; Schafer, B. W. S100 proteins: structure, functions and pathology. *Front. Biosci.* **2002**, *7*, 1356−1368.
(4) Castets, F.; Griffin, W. S.; Marks, A.; Van Eldik, L. J. Transcriptional regulation of the human S100 beta gene. *Mol. Brain Res.* **1997**, *46*, 208−216.
(5) Van Eldik, L. J.; Griffin, W. S. T. S100 beta expression in Alzheimer's disease: relation to neuropathology in brain regions. *Biochim. Biophys. Acta* **1994**, *1223*, 398−403.
(6) Mariggio, M. A.; Fulle, S.; Calissano, P.; Nicoletti, I.; Fano, G. The brain protein S-100ab induces apoptosis in PC12 cells. *Neuroscience* **1994**, *60*, 29−35.
(7) McLendon, R. E.; Vick, W. W.; Bigner, S. H.; Bigner, D. D. Monoclonal antibodies and diagnosis of brain neoplasms. *Cancer diagnosis in vitro using monoclonal antibodies*; Marcel Dekker: New York, 1988; pp 31−66.
(8) Camby, I.; Nagy, N.; Lopes, M. B.; Schafer, B. W.; Maurage, C. A.; et al. Supratentorial pilocytic astrocytomas, astrocytomas, anaplastic astrocytomas and glioblastomas are characterized by a differential expression of S100 proteins. *Brain Pathol.* **1999**, *9*, 1−19.
(9) Takahashi, K.; Yoshino, T.; Akagi, T.; Miyatani, K.; Hayashi, K.; et al. Natural killer (NK) activity of cultured S100 beta-positive T-leukemia cells. *Virchows Arch. B* **1990**, *59*, 159−164.
(10) Takashi, M.; Sakata, T.; Nakano, Y.; Yamada, Y.; Miyake, K.; et al. Elevated concentrations of the beta-subunit of S100 protein in renal cell tumors in rats. *Urol. Res.* **1994**, *22*, 251−255.
(11) Suzushima, H.; Asou, N.; Hattori, T.; Takatsuki, K. Adult T-cell leukemia derived from S100 beta positive double-negative (CD4-CD8-) T cells. *Leuk. Lymphoma* **1994**, *13*, 257−262.
(12) Garbe, C.; Leiter, U.; Ellwanger, U.; Blaheta, H. J.; Meier, F.; et al. Diagnostic value and prognostic significance of protein S-100beta, melanoma-inhibitory activity, and tyrosinase/MART-1 reverse transcription-polymerase chain reaction in the follow-up of high-risk melanoma patients. *Cancer* **2003**, *97*, 1737−1745.
(13) Jury, C. S.; McAllister, E. J.; MacKie, R. M. Rising levels of serum S100 protein precede other evidence of disease progression in patients with malignant melanoma. *Br. J. Dermatol.* **2000**, *143*, 269−274.
(14) Martenson, E. D.; Hansson, L. O.; Nilsson, B.; von Schoultz, E.; Mansson Brahme, E.; et al. Serum S-100b protein as a prognostic marker in malignant cutaneous melanoma. *J. Clin. Oncol.* **2001**, *19*, 824−831.
(15) Banfalvi, T.; Gilde, K.; Gergye, M.; Boldizsar, M.; Kremmer, T.; et al. Use of serum 5-S-CD and S-100B protein levels to monitor the clinical course of malignant melanoma. *Eur. J. Cancer* **2003**, *39*, 164−169.
(16) Guo, H. B.; Stoffel-Wagner, B.; Bierwirth, T.; Mezger, J.; Klingmuller, D. Clinical significance of serum S100 in metastatic malignant melanoma. [republished from *Eur. J. Cancer* 1995, *31A* (6) (June), 924−928] *Eur. J. Cancer* **1995**, *31A*, 1898−1902.
(17) Henze, G.; Dummer, R.; Joller-Jemelka, H. I.; Boni, R.; Burg, G. Serum S100−a marker for disease monitoring in metastatic melanoma. *Dermatology* **1997**, *194*, 208−212.
(18) Buer, J.; Probst, M.; Franzke, A.; Duensing, S.; Haindl, J.; et al. Elevated serum levels of S100 and survival in metastatic malignant melanoma. *Br. J. Cancer* **1997**, *75*, 1373−1376.
(19) Abraha, H. D.; Fuller, L. C.; Du Vivier, A. W.; Higgins, E. M.; Sherwood, R. A. Serum S-100 protein: a potentially useful prognostic marker in cutaneous melanoma. *Br. J. Dermatol.* **1997**, *137*, 381−385.
(20) Djukanovic, D.; Hofmann, U.; Sucker, A.; Rittgen, W.; Schadendorf, D. Comparison of S100 protein and MIA protein as serum marker for malignant melanoma. *Anticancer Res.* **2000**, *20*, 2203−2207.
(21) Schmitz, C.; Brenner, W.; Henze, E.; Christophers, E.; Hauschild, A. Comparative study on the clinical use of protein S-100B and MIA (melanoma inhibitory activity) in melanoma patients. *Anticancer Res.* **2000**, *20*, 5059−5063.
(22) Hansson, L. O.; von Schoultz, E.; Djureen, E.; Hansson, J.; Nilsson, B.; et al. Prognostic value of serum analyses of S-100 protein beta in malignant melanoma. *Anticancer Res.* **1997**, *17*, 3071−3073.
(23) Weber, D. J.; Rustandi, R. R.; Carrier, F.; Zimmer, D. B. *Interaction of dimeric S100B($\beta\beta$) with the tumor suppressor protein: A model for Ca-dependent S100-target protein interactions*; Kluwer Academic Publishers: Dordrecht, The Netherlands, 2000; pp 469−487.
(24) Rustandi, R. R.; Baldisseri, D. M.; Weber, D. J. Structure of the negative regulatory domain of p53 bound to S100B($\beta\beta$). *Nat. Struct. Biol.* **2000**, *7*, 570−574.
(25) Lin, J.; Blake, M.; Tang, C.; Zimmer, D.; Rustandi, R. R.; et al. Inhibition of p53 transcriptional activity by the S100B calcium-binding protein. *J. Biol. Chem.* **2001**, *276*, 35037−35041.
(26) Weber, D. J.; Markowitz, J.; Carrier, F.; MacKerell, A. D., Jr. Inhibitors of the S100-p53 Protein-Protein Interaction and Method of Inhibiting Cancer Employing the Same. In *United States Patent and Trademark Office*; University of Maryland, Baltimore: Baltimore, MD, 2003.
(27) Rustandi, R. R.; Drohat, A. C.; Baldisseri, D. M.; Wilder, P. T.; Weber, D. J. The Ca^{2+}-dependent interaction of S100B($\beta\beta$) with a peptide derived from p53. *Biochemistry* **1998**, *37*, 1951−1960.
(28) Wilder, P. T.; Rustandi, R. R.; Drohat, A. C.; Weber, D. J. S100B-($\beta\beta$) inhibits the protein kinase C-dependent phosphorylation of a peptide derived from p53 in a Ca-dependent manner. *Protein Sci.* **1998**, *7*, 794−798.
(29) Baudier, J.; Delphin, C.; Grundwald, D.; Khochbin, S.; Lawrence, J. J. Characterization of the tumor suppresor protein p53 as a protein kinase C substrate and a S100B-binding protein. *Proc. Natl. Acad. Sci. U.S.A.* **1992**, *89*, 11627−11631.
(30) Giaccia, A. J.; Kastan, M. B. The complexity of p53 modulation: emerging patterns from divergent signals. *Genes Dev.* **1998**, *12*, 2973−2983.
(31) Drohat, A. C.; Tjandra, N.; Baldisseri, D. M.; Weber, D. J. The use of dipolar couplings for determining the solution structure of rat apo-S100B. *Protein Sci.* **1999**, *8*, 800−809.
(32) Drohat, A. C.; Baldisseri, D. M.; Rustandi, R. R.; Weber, D. J. Solution structure of calcium-bound rat S100B($\beta\beta$) as determined by NMR spectroscopy. *Biochemistry* **1998**, *37*, 2729−2740.
(33) Gohlke, H.; Klebe, G. Approaches to the description and prediction of the binding affinity of small-molecule ligands to macromolecular receptors. *Angew. Chem., Int. Ed.* **2002**, *41*, 2644−2676.
(34) Stout, T. J.; Tondi, D.; Rinaldi, M.; Barlocco, D.; Pecorari, P.; Santi, D. V.; Kuntz, I. D.; Stroud, R. M.; Shoichet, B. K.; Costi, M. P. Structure-based design of inhibitors specific for bacterial thymidylate synthase. *Biochemistry* **1999**, *38*, 1607−1617.
(35) Li, R.; Chen, X.; Gong, B.; Selzer, P. M.; Li, Z.; Davidson, E.; Kurzban, G.; Miller, R. E.; Nuzum, E. O.; McKerror, J. H.; Fletterick, R. J.; Gillmor, S. A.; Craik, C. S.; Kuntz, I. D.; Cohen, F. E.; Kenyon, G. L. Structure-based design of parasitic protease inhibitors. *Bioorg. Med. Chem.* **1996**, *4*, 1421−1427.
(36) Schnecke, V.; Kuhn, L. A. Database Screening for HIV protease ligands: the influence of binding-site conformation and representation on ligand selectivity. *Proc. Int. Intell. Syst. Mol. Biol.* **1999**, 242−251.
(37) Selzer, P. M.; Chen, X.; Chan, V. J.; Cheng, M.; Kenyon, G. L.; Kuntz, I. D.; Sakanari, J. A.; Cohen, R. E.; McKerrow, J. H. Leishmania major: molecular modeling of cysteine proteases and prediction of new nonpeptide inhibitors. *Exp. Parasitol.* **1997**, *87*, 212−221.
(38) Tait, B. D.; Hagen, S.; Domagala, J.; Ellsworth, E. L.; Gajda, C.; Hamilton, H. W.; Prasad, J. V.; Ferguson, D.; Graham, N.; Hupe, D.; Nouhan, C.; Tummino, P. J.; Humblet, C.; Lunney,

E. A.; Pavlovsky, A.; Rubin, J.; Gracheck, S. J.; Baldwin, E. T.; Bhat, T. N.; Erikson, J. W.; Gulnik, S. V.; Liu, B. 4-Hydroxy-5,6-dihydropyrones. 2. Potent non-peptide inhibitors of HIV protease. *J. Med. Chem.* **1997**, *40*, 3781−3792.

(39) Mahajan, S.; Ghosh, S.; Sudbeck, E. A.; Zheng, Y.; Downs, S.; Hupke, M.; Uckun, F. M. Rational design and synthesis of a novel anti-leukemic agent targeting Bruton's tyrosine kinase (BTK), LFM-A13 [alpha-cyano-beta-hydroxy-beta-methyl-N-(2,5-dibromopheyl)propenamide. *J. Biol. Chem.* **1999**, *274*, 9587−9599.

(40) Sudbeck, E.; Liu, X. P.; Narla, R. K.; Mahajan, S.; Ghosh, S.; Mao, C.; Uckun, F. N. Structure-based design of specific inhibitors of Janus kinase 3 as apoptosis-inducing antileukemic agents. *Clin. Cancer Res.* **1999**, *5*, 1569−1582.

(41) Chen, I.-J.; Neamati, N.; Nicklaus, M. C.; Orr, A.; Anderson, L.; Barchi, J. J., Jr.; Kelly, J. A.; Pommier, Y.; MacKerell, A. D., Jr. Identification of HIV-1 integrase inhibitors via three-dimensional database searching using ASV and HIV-1 integrases as targets; *Biorg. Med. Chem.*, in press.

(42) Tracy, J. W.; Webster, L. T. Drugs used in the chemotherapy of protozoal infections. *Goodman & Gilman's The Pharmacological Basis of Therapeutics*, 10th ed.; McGraw-Hill Companies: New York, 2001; pp 1109−1111.

(43) Kuntz, I. D.; Blaney, J. M.; Oatley, S. J.; Langridge, R.; Ferrin, T. E. A Geometric Approach to Macromolecule-Ligand Interactions. *J. Mol. Biol.* **1982**, *161*, 269−288.

(44) Ewing, T. J. A.; Kuntz, I. D. Critical Evaluation of Search Algorithms Used in Automated Molecular Docking. *J. Comput. Chem.* **1997**, *18*, 1175−1189.

(45) Pan, Y.; Huang, N.; Cho, S.; MacKerell, A. D., Jr. Consideration of molecular weight during compound selection in virtual target-based database screening. *J. Chem. Inf. Comput. Sci.* **2003**, *43*, 267−272.

(46) Chen, I.-J., Neamati, N., MacKerell, A. D., Jr. Structure-Based Inhibitor Design Targeting HIV-1 Integrase. *Curr. Drug Targets: Infect. Disord.* **2002**, *2*, 217−234.

(47) Inman, K. G.; Yang, R.; Rustandi, R. R.; Miller, K. E.; Baldisseri, D. M.; et al. Solution NMR structure of S100B bound to the high-affinity target peptide TRTK-12. *J. Mol. Biol.* **2002**, *324*, 1003−1014.

(48) Leach, A. R.; Kuntz, I. D. Conformational analysis of flexible ligands in macromolecular receptor sites. *J. Comput. Chem.* **1992**, *13*, 730−748.

(49) Ferrin, T. E.; Huang, C. C.; Jarvis, L. E.; Landridge, R. The MIDAS Display System. *Mol. Graphics* **1988**, *6*, 13−27.

(50) Desjarlais, R. L.; Sheridan, R. P.; Dixon, J. S.; Kuntz, I. D.; Venkataraghaven, R. Docking Flexible Ligands to Macromolecular Receptors by Molecular Shape. *J. Med. Chem.* **1986**, *29*, 2149−2153.

(51) Kuntz, I. D.; Meng, E. C.; Schoichet, B. K. Structure-Based Molecular Design. *Acc. Chem. Res.* **1994**, *27*, 117−123.

(52) Goodford, P. J. A Computational Procedure for Determining Energetically Favorable Binding Sites on Biologically Important Macromolecules. *J. Med. Chem.* **1984**, *28*, 849−857.

(53) Meng, E. C.; Shoichet, B. K.; Kuntz, I. D. Automated Docking with Grid-Based Energy Evaluation. *J. Comput. Chem.* **1992**, *13*, 505−524.

(54) Butina, D. Unsupervised data base clustering on daylight's fingerprint and Tanimoto similarity: a fast and automated way to cluster small and large data sets. *J. Chem. Inf. Comput. Sci.* **1999**, *39*, 747−750.

(55) Bagby, S.; Tong, K. I.; Ikura, M. Optimization of protein solubility and stability for protein nuclear magnetic resonance. *Methods Enzymol.* **2001**, *339*, 20−41.

(56) Jenkins, T. C.; Lane, A. N. AT selectivity and DNA minor groove binding: modelling, NMR and structural studies of the interactions of propamidine and pentamidine with d(CGCGAATTCGCG)2. *Biochim. Biophys. Acta* **1997**, *1350*, 189−204.

(57) Morgan, D. M. Tetrazolium (MTT) assay for cellular viability and activity. *Methods Mol. Biol.* **1998**, *79*, 179−183.

(58) Delaglio, F.; Grzesiek, S.; Vuister, G. W.; Zhu, G.; Pfeifer, J.; et al. NMRPipe: a multidimensional spectral processing system based on UNIX pipes. *J. Biomol. NMR* **1995**, *6*, 277−293.

(59) Johnson, M. A.; Rotondo, A.; Pinto, B. M. NMR studies of the antibody-bound conformation of a carbohydrate-mimetic peptide. *Biochemistry* **2002**, *41*, 2149−2157.

(60) Mori, S.; Abeygunawardana, C.; Johnson, M. O.; van Zijl, P. C. Improved sensitivity of HSQC spectra of exchanging protons at short interscan delays using a new fast HSQC (FHSQC) detection scheme that avoids water saturation. *J. Magn. Reson. B* **1995**, *108*, 94−98.

(61) Spera, S.; Bax, A. Empirical correlation between protein backbone conformation and Cα and Cβ/13-C nuclear magnetic resonance chemical shifts. *J. Am. Chem. Soc.* **1991**, *113*, 5490−5492.

(62) Live, D. H.; Davis, D. G.; Agosta, W. C.; Cowburn, D. Longe range hydrogen bond mediated effects in peptides: ^{15}N NMR study of gramicidin S in water and organic solvents. *J. Am. Chem. Soc.* **1984**, *106*, 1939−1941.

(63) Edison, A. S.; Abildgaard, F.; Westler, W. M.; Mooberry, E. S.; Markley, J. L. Practical introduction to theory and implementation of multinuclear, multidimensional nuclear magnetic resonance experiments. *Methods Enzymol.* **1994**, *239*, 3−79.

(64) Mayer, M.; Meyer, B. Group epitope mapping by saturation transfer difference NMR to identify segments of a ligand in direct contact with a protein receptor. *J. Am. Chem. Soc.* **2001**, *123*, 6108−6117.

(65) Yan, J.; Kline, A. D.; Mo, H.; Shapiro, M. J.; Zartler, E. R. The effect of relaxation on the epitope mapping by saturation transfer difference NMR. *J. Magn. Reson.* **2003**, *163*, 270−276.

(66) Piotto, M.; Saudek, V.; Sklenar, V. Gradient-tailored excitation for single-quantum NMR spectroscopy of aqueous solutions. *J. Biomol. NMR* **1992**, *2*, 661−665.

(67) Scott, K.; Stonehouse, J.; Keeler, J.; Hwang, T. L.; Shaka, A. J. *J.Am. Chem. Soc.* **1995**, *117*, 4199−4200.

(68) Bax, A.; Davis, A. L. *J. Magn. Reson.* **1985**, *65*, 355−360.

(69) Jeener, J.; Meier, B. H.; Bachmann, P.; Ernst, R. R. Investigation of exchange processes by two-dimensional NMR. *J. Chem. Phys.* **1979**, *71*, 4546−4553.

(70) Bax, A.; Marion, D. *J. Biomol. NMR.* **1988**, *78*, 186−191.

(71) Bax, A.; Summers, M. F. *J. Am. Chem. Soc.* **1986**, *108*, 2093−2094.

(72) Weber, D. J.; Gittis, A. G.; Mullen, G. P.; Abeygunawardana, C.; Lattman, E. E.; et al. NMR docking of a substrate into the X-ray structure of staphylococcal nuclease. *Proteins* **1992**, *13*, 275−287.

(73) Weber, D. J.; Libson, A. M.; Gittis, A. G.; Lebowitz, M. S.; Mildvan, A. S. NMR docking of a substrate into the X-ray structure of the Asp-21 → Glu mutant of staphylococcal nuclease. *Biochemistry* **1994**, *33*, 8017−8028.

(74) Kleywegt, F. J.; Jones, T. A. Model-building refinement practice. *Methods Enzymol.* **1997**, *277*, 208−230.

(75) Schwieters, C. D.; Kuszewski, J. J.; Tjandra, N.; Marius Clore, G. The Xplor-NIH NMR molecular structure determination package. *J. Magn. Reson.* **2003**, *160*, 65−73.

(76) Schwieters, C. D.; Clore, G. M. The VMD-XPLOR visualization package for NMR structure refinement. *J. Magn. Reson.* **2001**, *149*, 239−244.

(77) Kraulis, P. J. MOLSCRIPT: a program to produce both detailed and schematic plots of protein structures. *J. Appl. Crystallogr.* **1991**, *24*, 946−950.

(78) Hajduk, P. J.; Meadows, R. P.; Fesik, S. W. Discovering high-affinity ligands for proteins. *Science* **1997**, *278*, 497−499.

(79) Fesik, S. W. NMR structure-based drug design. *J. Biomol. NMR* **1994**, *3*, 261−269.

(80) Wüthrich, K. *NMR of proteins and nucleic acids*; John Wiley: New York, 1986.

JM0497038